Power Flow Stabilization and Control of Microgrid with Wind Generation by Superconducting Magnetic Energy Storage

Marcelo Gustavo Molina, *Member, IEEE*, and Pedro Enrique Mercado, *Senior Member, IEEE*

***Abstract*—High penetration of renewable energy sources such as wind generation in microgrids (MGs) causes fluctuations of power flow and significantly affects the power system (PS) operation. This can lead to severe problems, such as system frequency oscillations, and/or violations of power lines capability. With the proper control, superconducting magnetic energy storage (SMES) is able to significantly enhance the dynamic security of the PS. In an SMES system, the power conditioning system (PCS) is the crucial component that directly influences the validity of the SMES in the dynamic control of the PS. This paper proposes the use of an improved SMES controller for the stabilization and control of the power flow of wind-hybrid MGs. In this sense, the design and implementation of a novel high-performance PCS scheme of the SMES is described. Moreover, a detailed model of the SMES unit is derived and a novel three-level control scheme is designed, comprising a full decoupled current control strategy in the *d–q* reference frame and an enhanced PS frequency controller. The dynamic performance of the proposed systems is fully validated by computer simulation.**

***Index Terms*—Distributed energy storage, microgrids (MGs), power conditioning system (PCS), superconducting magnetic energy storage (SMES).**

I. Introduction

DISTRIBUTED generation (DG) is presently emerging as a new paradigm to produce in situ highly reliable and good quality electrical power. Thus, DG systems are arising as an appropriate way to offer highly reliable, also called premium, electrical power supply to customers. In such systems, every unit must be able to operate independently without intercommunication due to the long distance between them. The greatest potential market for DG is displacing power supplied through the grid; thus bypassing congestion in existing transmission systems. On-site production minimizes transmission and distribution losses as well as transmission and distribution costs, a significant part of the total electricity cost [1]. In this sense, the most promising novel network structure that would allow obtaining a better use of distributed energy resources (DERs) is the electrical microgrid (MG). This new concept tackles all DERs as a unique subsystem, including DG, renewable energy sources (RESs), distributed energy storage (DES), and demand response (DR), and offers significant control capacities on its operation. This electrical grid can be managed as if were a group with predictable generation and demand, and can be operated as much interconnected to the main power system (PS) as autonomously isolated [2], [3]. In this way, flexible MGs can not only import and export energy to the main grid but also can operate in grid-connected or in island modes.

MGs are becoming a reality in a scenario in which RESs, DG, and DES systems can be conjugated and integrated into the grid. These concepts are growing in importance due not only to environmental aspects but also to social, economical, and political interests [4]. Moreover, the requirement for more flexible electric systems, changing regulatory and economic scenarios, and energy saving are providing especial impetus to the development of MGs. For MGs to work properly, an upstream interconnection switch must open typically during an unacceptable power quality condition, and the DER must be able to provide electrical power to the islanded loads. This includes maintaining appropriate voltage and frequency levels for the islanded subsystem. In this way, the DER must be able to supply the active and reactive power requirements during islanded operation, so that fast-acting generation reserve is needed. As a result, for stable operation to balance any instantaneous mismatch in active power, efficient DES must be used [5]–[7].

Nowadays, grid integration of wind power generation is becoming the most important and fastest growing form of electricity generation among renewable energies [8]. However, wind power frequently changes and is hardly predictable. The high penetration of wind power with abrupt changes adversely affects PS operation and can lead to severe problems, such as system frequency oscillations, and/or violations of power lines capability [9], [10]. To overcome these problems, superconducting magnetic energy storage (SMES) can be utilized as an effective DES device with the ability to rapidly and flexibly exchange power with the MG. The most important advantages of SMES devices include: high power and energy density with outstanding conversion efficiency, and fast and independent power response in four quadrants [11]. In an SMES system, the power conditioning system (PCS) is the interface that allows the effective connection to the PS. The dynamics of the PCS directly influences the validity of the SMES in the dynamic control of the PS.

Manuscript received July 1, 2010; revised September 29, 2010; accepted November 26, 2010. Date of current version May 13, 2011. This work was supported in part by the Argentinean National Agency for the Promotion of Science and Technology (ANPCyT) under Grant Proyecto de Investigación Científica y Tecnológica (PICT) 2005, 33407. Recommended for publication by Associate Editor G. Asher.

The authors are with the Argentinean National Council for Science and Technology Research (CONICET), CP C1033AAJ, Cdad. de Buenos Aires, Argentina, and also with the National University of San Juan (UNSJ), San Juan J5400ARL, Argentina (e-mail: mgmolina@ieee.org; pmercado@ieee.org).

Color versions of one or more of the figures in this paper are available online at http://ieeexplore.ieee.org.

Digital Object Identifier 10.1109/TPEL.2010.2097609

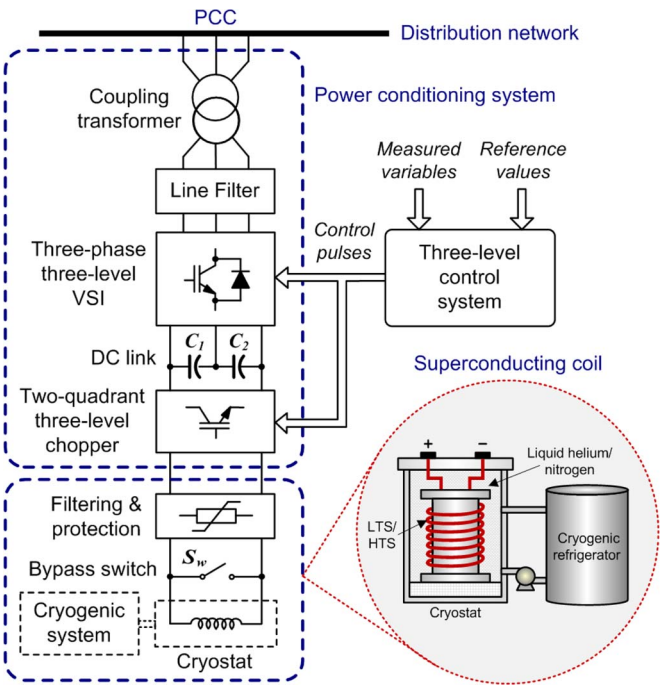

Fig. 1. General components of the proposed SMES unit.

With the appropriate topology of the PCS and its control system design, the SMES unit is capable of simultaneously performing both instantaneous active and reactive power flow control, and thus is able to dramatically enhance the MG dynamic security [12].

This paper proposes the use of an improved SMES controller for the stabilization and control of the power flow of hybrid MGs incorporating RESs such as wind generation. In this sense, the design and implementation of a novel high-performance PCS scheme of the SMES is described. A detailed model of the SMES unit is derived, including two power converters to provide the high-efficiency PCS capability and the superconducting coil (SC), as depicted in Fig. 1. The PCS consists of a three-phase three-level ac/dc converter and incorporates a two-quadrant three-level dc/dc converter as interface with the SMES coil. Moreover, based on the state-space averaging method a three-level control scheme is designed, comprising a full decoupled current control strategy in the synchronous-rotating $d-q$ reference frame with a novel controller to prevent the voltage drift/imbalance of the inverter dc-bus capacitors and an enhanced PS frequency controller. The dynamic performances of the proposed systems are fully validated by digital simulation carried out by using SimPowerSystems (SPS) of MATLAB/Simulink.

II. Application of SMES Systems in MGs

High power and energy density with outstanding conversion efficiency, and fast and independent power response in four quadrants makes SMES capable of providing significant benefits to many potential MG applications. Most of these SMES technology applications are described below.

1) *Distributed energy storage:* SMES units could provide the potential for energy storage of up to several MWh with a high efficiency (up to 95%) and a rapid response (in milliseconds). This aspect makes them ideal for energy management with large variations in energy requirements, as well as for backup power supply in case of loss of the utility main power supply or as a replacement of some generating units in the MG.
2) *Spinning reserve:* In case of contingencies, such as failures of generating units or other MG components, a certain amount of short-term generation must be kept unloaded as spinning reserve. This reserve must be appropriately activated by means of the primary frequency control (PFC). SMES systems can be effectively used in order to store excess energy during off-peak periods for substituting the generation reserve during the action of the PFC, and thus, for enhancing the dynamic security of the MG.
3) *Load following:* An SMES device has the ability to follow system load changes almost instantaneously that allows for conventional generating units to operate at constant output power.
4) *MG stability:* An SMES unit has the capability to damp out low frequency power oscillations and to stabilize the system frequency as a result of system transients. Since a SMES is capable of controlling both the active and reactive powers simultaneously, it can act as a good device in order to stabilize the MG with high level of penetration of RESs, such as photovoltaic or particularly wind generation.
5) *Automatic generation control (AGC):* An SMES unit can be used as a controlling function in an AGC system to support a minimum of area control error (ACE).
6) *Tie-line power flow stabilization and control:* A schedule of power between various MGs or control areas inside the same MG requires that actual net power matches closely with the scheduled power. Unfortunately, generators with highly fluctuating active power profile in one MG produce an error in the actual power delivered respect to the scheduled one, which can result in inefficient use of generation and system components. SMES can be designed with appropriate controls to provide power in order to nearly eliminate this error and to ensure that generation is efficiently used and power schedules are met.
7) *Power quality improvement:* SMES can provide ride through capabilities and smooth out disturbances on the MG that would otherwise interrupt sensitive customer loads. These devices have very fast response and can inject active power in less than one power cycle; thus providing premium power supply to critical customers and preventing from losing power.
8) *Reactive power flow control and power factor correction:* An SMES is capable of controlling the generated reactive power simultaneously and independently of the active power, which enables the correction of the power factor.
9) *Voltage control:* SMES systems have shown to be effective for providing voltage support and regulation by locally generating reactive power.

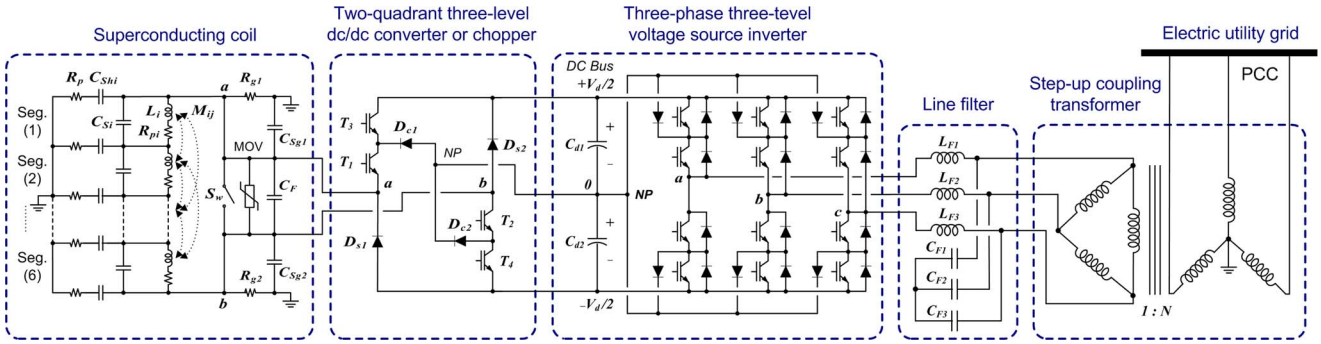

Fig. 2. Detailed model of the proposed SMES system, including the PCS and the SC.

III. Modeling of the Proposed SMES System

Fig. 2 summarizes the proposed detailed model of the SMES controller for applications in the distribution network level. This model consists of the PCS and the SMES coil with its filtering and protection system.

A. Power Conditioning System

The PCS provides a power electronic interface between the electrical MG and the SC, aiming at achieving two goals: one is to convert electric power from dc to ac, and the other is to charge/discharge (Ch/Dsch) efficiently the SC. The major component of the proposed PCS is the well-known three-phase voltage source inverter (VSI) or converter (VSC) shunt-connected to the distribution network by means of a coupling step-up Δ–Y coupling transformer and the corresponding line sinusoidal filter [13], [14], as described in Fig. 2 (right side). The VSI corresponds to a dc/ac static converter using high-power fast isolated gate bipolar transistors (IGBTs) as main power switches. This semiconductor device is employed due to its lower switching losses and reduced size when compared to other devices. In addition, as the power rating of the inverter is lesser than a few MWs for a modern DER application, the output voltage control of the VSI can be efficiently achieved through sinusoidal pulsewidth modulation (SPWM) techniques.

The proposed inverter structure is based on a diode-clamped three-level topology, also called neutral point clamped (NPC), instead of a standard two-level six-pulse inverter structure. This three-level twelve-pulse VSI topology generates a more smoothly sinusoidal output voltage waveform than conventional structures without increasing the switching frequency and effectively doubles the power rating of the VSI for a given semiconductor device [15]. In this way, the three-level pole attempts to address some limitations of the standard two-level [16] by offering an additional flexibility of a level in the output voltage, which is used to assist in the output waveform structure, so that not only the harmonic performance of the inverter is improved, but also the efficiency and reliability of the system. By increasing the number of levels in the converter, the output voltages waveforms have more steps generating a staircase approximation of a sinusoidal waveform, which has a reduced harmonics distortion. However, this topology has the drawback of having voltage imbalance problems between the VSI dc-link capacitors when active power flow is exchanged with utility grid and auxiliary converters should be used in order to provide a compensating power flow between both capacitors of the dc link [17]. Moreover, a high number of levels increases the control complexity and introduces voltage clamping requirements, circuit layout, and packaging constraints.

The inclusion of an SMES coil into the dc bus of the VSI demands the use of an improved interface to adapt the wide range of variation in voltage and current levels between both devices. Controlling the SMES coil rate of Ch/Dsch requires varying as much the coil voltage magnitude as the polarity according to the coil state-of-charge, while keeping essentially constant and balanced the voltage of the inverter dc-link capacitors [18]. To this aim, a new two-quadrant three-level IGBT dc/dc converter or chopper is proposed to be employed in this work, as shown in Fig. 2 (left side). This converter allows decreasing the ratings of the overall PCS (specifically the VSI and transformer) by regulating the current flowing from the SMES coil to the inverter of the VSI and vice versa. Major advantages of the three-level dc/dc chopper topologies compared to traditional two-level ones [19], [20] include reduction of voltage stress of each IGBT by half, permitting to increase the chopper power ratings while maintaining high dynamic performance and decreasing the harmonics distortion produced. Furthermore, it includes the availability of redundant switching states, which allow generating the same output voltage vector through various states. This last feature is very significant to reduce switching losses and VSI dc current ripple, but mainly to maintain the charge balance of the dc-bus capacitors, thus avoiding contributing to the ac system with additional distortion.

Table I lists all possible combinations of the chopper output voltage vectors, V_{ab} (defining the SMES side of the circuit as the output side) and their corresponding IGBT switching states. As derived, the chopper can be thought of as a switching matrix device that combines various states for applying either a positive, negative or null voltage to the SC coil. The addition of an extra level to the dc/dc chopper allows enlarging its degrees of freedom. As a result, the charge balance of the dc-bus capacitors can be controlled by using the extra switching states, at the same time acting as an enhanced conventional dc/dc converter. The output voltage vectors can be selected based on the required SMES coil voltage and dc-bus neutral point (*NP*) voltage. In this way, multiple subtopologies can be used in order to

TABLE I
THREE-LEVEL CHOPPER OUTPUT VOLTAGE VECTORS AND THEIR CORRESPONDING IGBT SWITCHING STATES

States	T_1	T_2	T_3	T_4	V_{ab}
1	1	1	1	1	$+V_d$
2	0	0	0	0	$-V_d$
3	0	1	0	1	*0*
4	1	0	1	0	*0*
5	1	1	0	0	*0*
6	1	1	0	1	$+V_d/2$
7	1	1	1	0	$+V_d/2$
8	1	0	0	0	$-V_d/2$
9	0	1	0	0	$-V_d/2$

obtain output voltage vectors of magnitude 0 and $V_d/2$, in such a way that different vectors of magnitude $V_d/2$ produce opposite currents flowing from/to the neutral point. This condition causes a fluctuation in the *NP* potential that permits to maintain the charge balance of the dc-link capacitors. By properly selecting the duration of the different output voltage vectors, an efficient dc/dc controller with *NP* voltage control capabilities is obtained.

The dc/dc chopper has basically three modes of operation, namely the buck or charge mode, the standby or free-wheeling mode and the boost or discharge mode. These modes are obtained in this work by using a buck-boost topology control mode contrary to a bang-bang control mode [21], which is much simpler yet produces higher ac losses in the SC. The behaviour of the chopper for each mode of operation can be explained in terms of operating a combination of three of the switching states shown in Table I during a switching cycle T_s. The purpose of the chopper is to apply a positive, null, or negative average voltage to the SMES coil, according to the mode of operation.

In the first mode of operation, that is the charge mode, the chopper works as a step-down (buck) converter. Since power is supplied to the SC from the MG, this mode can also be called powering mode, and makes use of a combination of positive and null vectors. This is achieved through the switching states 1, 5, and 6 or 7 in order to produce output voltage vectors $+V_d$, 0 and $+V_d/2$ with different contribution of charge at the NP from capacitors C_{d1} and C_{d2}. In this way, only subtopologies closest to the state 1 are used. In consequence, only one semiconductor device is switched per switching cycle; this reducing the switching losses compared to the standard two-level converter, and thus, also reducing the input/output current ripple.

Once completed the charging of the SMES coil, the operating mode of the converter is changed to the standby mode, for which only the state 5 is used. Thus, the SMES coil current circulates in a closed loop, so that this mode is also known as free-wheeling mode, and the current remains fairly constant. In fact, operating losses as conduction power losses of IBGTs T_1 and T_2 occurs in this free-wheeling mode, and are considerably higher than ac losses produced inside the superconducting magnet during the SMES operation (charge and discharge modes). These losses into the SC are a consequence of variations of the coil current (and magnetic field), which produce eddy currents and magnetization losses (typically less than 20 W/s for a 0.2-MVA/5-MJ SMES at less than 20 K).

In the third mode of operation, i.e., the discharge mode, the chopper works as a step-up (boost) converter. Since power is returned back from the SC to the electric grid, this mode can also be called regenerative mode, and makes use of a combination of negative and null vectors. This is achieved through the switching states 2, 5 and 8 or 9 in order to produce output voltage vectors $-V_d$, 0, and $-V_d/2$ with independent contribution of charge at the *NP* from capacitors C_{d1} and C_{d2}. In this way, only subtopologies closest to the state 2 are used; consequently only one semiconductor device is switched per switching cycle in the same way as the charge mode.

B. SMES Coil

An SMES system consists of several sub-systems, which must be carefully designed in order to obtain a high-performance compensation device. The base of the SMES unit is a large superconducting coil (SC), whose basic structure is composed of the cold components itself (the SC with its support and connection components, and the cryostat) and the cryogenic refrigerating system, as shown at the bottom side in Fig. 1.

The equivalent circuit of the SMES coil makes use of a lumped parameters network represented by a six-segment model comprising self inductances (L_i), mutual couplings between segments (i and j, M_{ij}), ac loss resistances (R_{si}), skin effect-related resistances (R_{pi}), turn-ground (shunt—C_{Shi}), and turn–turn capacitances (series—C_{Si}), as depicted at the left side of Fig. 2. This model is based on the ones previously proposed in [22], [23], and is reasonably accurate for electric systems transients studies, over a frequency range from dc to several thousand Hertz. The inclusion of surge capacitors (C_{Sg1} and C_{Sg2}) and a filter capacitor C_F in parallel with grounding-balance resistors (R_{g1} and R_{g2}) allows reducing the effect of resonances. A metal oxide semiconductor (MOV) protection for transient voltage surge suppression is included between the SMES model and the dc/dc converter.

IV. PROPOSED CONTROL SCHEME OF THE SMES SYSTEM

The proposed hierarchical control scheme of the SMES unit consists of an external, middle, and internal level. Its design is based on concepts of instantaneous power on the synchronous-rotating *d–q* reference frame [24], [25]. This structure has the goal of rapidly and simultaneously controlling the active and reactive power flow provided by the SMES. To this aim, the controller must ensure the instantaneous energy balance among all the SMES components. In this way, the stored energy is regulated through the PCS in a controlled manner for achieving the charging and discharging of the SC coil.

A. External-Level Control

The external-level control, which is outlined in Fig. 3, is responsible for determining the active and reactive power exchange between the SMES and the MG. This control strategy is designed for performing two major high-priority control

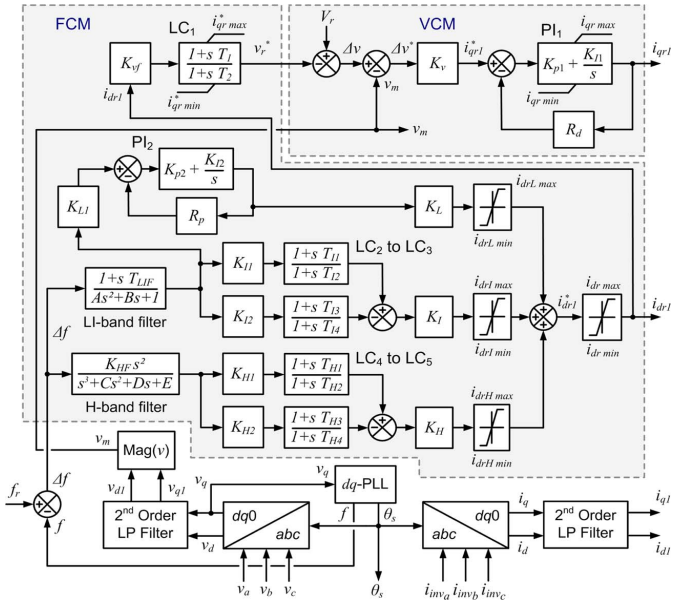

Fig. 3. General structure of the external-level control of the SMES system.

objectives: the voltage control mode (VCM) with only reactive power compensation capabilities (case of a traditional static synchronous compensator with no ESS), and the frequency control mode (FCM) with both active and reactive power exchange capabilities aiming at controlling (regulating and supporting) the PS frequency (case of an SMES operating as a stabilization device).

The standard control loop of the external level is the VCM [26] and consists in controlling the voltage at the point of common coupling (PCC) of the SMES to the distribution feeder of the MG through the modulation of the reactive component of the VSI output current, i_{q1}. This control mode has proved a very good performance in conventional static var compensators (with no energy storage). In this work, this control mode is subordinated to the FCM when the device is used as a power stabilizer. The design of this control loop in the rotating frame is simpler than using stationary frame techniques, and employs a standard proportional–integral (PI) compensator including an antiwindup system to enhance the dynamic performance of the VCM system. This mode compares the reference voltage V_r set by the SMES operator with the actual measured value at the PCC (v_m) in order to eliminate the steady-state voltage offset via the PI compensator. A voltage regulation droop R_d (typically 5%) is included in order to allow the terminal voltage of the VSI to vary in proportion with the compensating reactive current. Thus, the PI controller with droop characteristics becomes a simple phase-lag compensator, resulting in a stable fast response compensator. This feature is particularly significant in cases that more high-speed voltage compensators are operating in the area. This characteristic is comparable to the one included in conventional generators' voltage regulators.

The FCM is the highest priority control mode that aims at controlling the MG frequency through the modulation of both, the reactive component of the output current i_q (as a conventional var compensator) and the active component i_d (case of an SMES). In the case of controlling i_q, the set point of the lower priority VCM, i.e., the voltage reference signal V_r, is adjusted with a stabilizing voltage signal proportional to Δf (defined as $f_r - f$), which directly represents the power oscillation of the PS. This added signal causes the output quadrature current of the VSI i_q to vary around the operating point defined by V_r, the purpose of this variation being to improve the damping of the power oscillations. In this way, the voltage at the PCC is forced to decrease when the frequency deviation Δf is positive aiming at reducing the transmitted power through the distribution system, and thus, providing an effective fast-acting voltage reduction reserve that opposes the deceleration of generators in the MG. This action is performed in the opposite way when the frequency deviation Δf is negative, and then generators accelerate. A lag-compensator is used to assist in shaping the gain and phase characteristics of the frequency stabilizer for the case of modulating the VSI output quadrature current.

Although the power oscillation damping approach of the standard var compensator is rather effective, the most effective compensation action for power oscillations damping, and thus, for PFC is carried out by rapidly exchanging active power with the utility system, that is to say by controlling the output direct current of the SMES i_d. Considering this case, as in the previous case, the reference of the SMES device output direct current, i_{dr}, is directly derived from Δf. Since a robust and efficient frequency control scheme requires the effective damping of a wide range of generators power oscillations, ranging from less than 0.2 Hz for global oscillations to 4 Hz for local oscillations of microgeneration units, a flexible multiband structure (MBS) controller is proposed in this work [27]. Despite the potential of modern control techniques with different structures (adaptive control, neural networks, fuzzy control, etc.), PS utilities still prefer the fixed structure controller. In this way, the novel proposed controller architecture, presents several degrees of freedom for achieving a robust tuning over a wide range of frequencies while keeping the same structure. The basic idea is to separate the frequency spectra in two decoupled bands for covering small signal frequency disturbances: the intermediate band is used for interarea modes usually found in the range of 0.2–1.0 Hz and the high band deals with local modes, either plant or intermachines, with a typical frequency range of 0.8–4.0 Hz. Appropriate damping of power swings in both spectral bands require from the controller a frequency response with an increasing gain from low to high bands and phase leading in the whole range of action. This condition is achieved by employing differential filters synthesized through lead–lag compensators, providing intrinsic dc wash out, zero gain at high frequency, and phase leading up to the resonant frequency. Thus, the two resulting compensators are superposed in order to obtain a combined frequency stabilizer with an adequate phase characteristic for all small frequency deviation modes.

In the case of large signal frequency disturbances, characterized by common modes in the frequency range below 0.1 Hz, the controller experiences new constraints. Since the SMES participates of the MG PFC, the gain needed for the low frequency band is lower than the previous two cases and roughly constant

for all the spectral band of interest, which extends from near dc to 0.1 Hz. A speed-droop R_p (typically 5%) is also necessary to be included in order to obtain a stable load division among several fast-response devices operating in parallel. This characteristic is analogous to the one included in conventional generator speed governors. As a result, the PI controller with droop characteristics becomes a simple phase-lag compensator that ensures an effective positive damping while maintaining performance and robustness in the intermediate and high bands.

This frequency compensator structure controls the rapid active power exchange between the SMES and the MG, forcing the SMES coil to absorb active power when generators accelerate (charge mode), or to inject active power when they decelerate (discharge mode). This global architecture ensures almost the same good performance in damping power oscillations at all modes of interest. The resulting stabilizer signal composed from all bands is passed through a final limiter for setting the reference i_{dr}. An input frequency filter is used for processing the frequency deviation signal Δf obtained from the phase locked loop (PLL). The filter is associated with the low and intermediate bands, and guarantees a plane response in the 0 to 4.0 Hz range. In all cases, the frequency signal is derived from the positive sequence components of the ac voltage vector measured at the PCC of the SMES, through a PLL. The design of the PLL is based on concepts of instantaneous power theory in the *dq* reference frame. This device also synchronizes, by providing the phase θ_s, the coordinate transformations from *abc* to *dq* components in the voltage and current measurement system. These signals are then filtered by using second-order low-pass filters in order to obtain the fundamental components employed in the control system.

B. Middle-Level Control

The middle-level control makes the expected output, i.e., positive sequence components of i_d and i_q, to dynamically track the reference values set by the external level. The middle-level control design, which is depicted in Fig. 4, is based on a linearization of the state-space averaged model of the PCS inverter in *d–q* coordinates described in-depth in [13]. Inspection of this model shows a cross-coupling of both components of the SMES VSI output current through the synchronous angular speed of the grid voltage at the fundamental frequency. Therefore, in order to achieve a fully decoupled active and reactive power control, it is simply required to decouple the control of i_d and i_q through two conventional PI controllers, PI_3 and PI_4. In addition, the model exhibits an additional coupling resulting from the dc capacitors voltage V_d as much in the dc side as in the ac side of the PCS [26], [28]. This difficulty demands to maintain the dc-bus voltage as constant as possible in order to decrease the influence of the dynamics of V_d. The solution to this problem is obtained by using another PI controller (PI_3) that allows eliminating the steady-state voltage variations at the dc bus, by forcing the instantaneous balance of power between the dc and the ac sides of the PCS inverter through the modulation of the duty cycle D of the three-level dc/dc chopper. Thus, the converter control is designed by computing the duty cycle of the

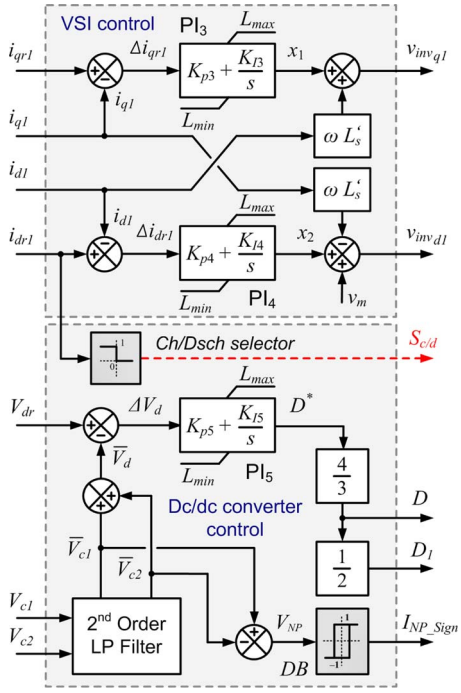

Fig. 4. General scheme of the middle-level control of the SMES system.

chopper semiconductors for the required stiff voltage at the dc bus according to the mode of operation of the dc/dc converter (Ch/Dsch) via a corrective action of integral-type (controller PI_5) [29]. Therefore, dc-bus voltage deviations, caused by actual VSI switching losses and capacitors power losses can be quickly counteracted. A Ch/Dsch mode selector is used from the required instantaneous actual output current of the SMES $i_{dr\,1}$ in order to determine the operation of the converter through the signal $S_{c/d}$. Finally, duty cycles D_1 and D_2 are computed through the novel controller in order to prevent dc-bus capacitors voltage drift/imbalance, as formerly explained. This novel extra dc voltage control block provides the availability of managing the redundant switching states of the chopper according to the capacitors charge unbalance measured through the neutral point voltage, V_{NP}. This specific loop modifying the modulating waveforms of the internal-level control is also proposed for reducing instability problems caused by harmonics as much in the SMES device as in the MG. The application of a static determination of D_1 and D_2, such as the case of $D_1 = D_2 = D/2$, has proved to be good enough for reaching an efficient equalization of the dc-bus capacitors over the full range of VSI output voltages and active/reactive power requirements.

C. Internal-Level Control

Fig. 5 shows a basic scheme of the internal-level control of the SMES unit. The internal level provides dynamic control of input signals for the dc/ac and dc/dc converters. This level is responsible for generating the triggering control signals for the twelve valves of the three-level VSI, according to the modulation techniques (SPWM) [30] and types of semiconductors (IGBTs)

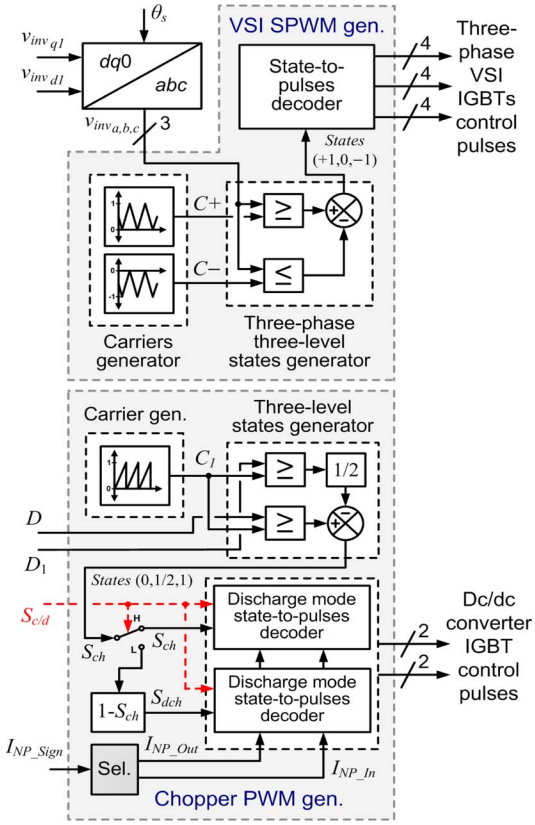

Fig. 5. Structure of the internal-level control of the SMES system.

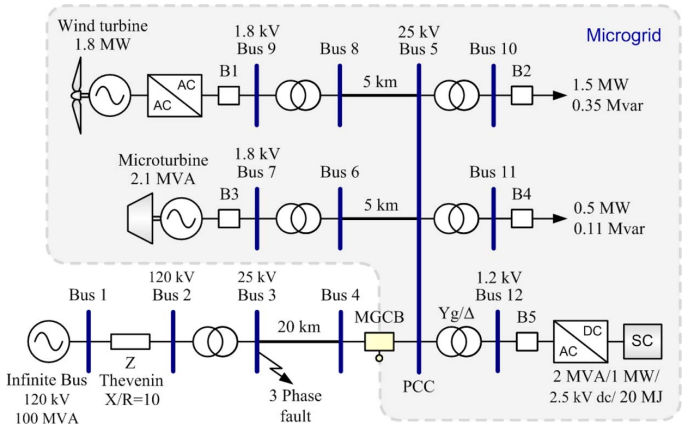

Fig. 6. Single-line diagram of the test PS with the proposed MG.

used and for the four IGBTs of the buck/boost three-level dc/dc converter.

In the case of the sinusoidal PWM pulses generator block, the controller of the VSI generates pulses for the carrier-based three-phase PWM inverter using the three-level topology. Thus, the expected sinusoidal-based output voltage waveform $v_{\rm inv}$ of the SMES, which is derived from the coordinate transformation from *dq* components provided by the middle-level control, is compared to two positive and negative triangular signals generated by the carriers generator for producing three-state SPWM vectors (1, 0, −1). These states are decoded by the states-to-pulses decoder via a look-up-table that relates each state with the corresponding firing pulse for each IGBT of the four ones in each leg of the three-phase three-level VSI.

In the case of the dc/dc converter firing pulses generator block, the three-level PWM modulator is built using a compound signal obtained as the difference of two standard two-level PWM signals. According to the mode of operation of the chopper (Ch/Dsch), the consequent three-state PWM vectors (0, 1/2, 1) are synthesized. Two direct 2-D lookup tables are employed for relating each state with the corresponding firing pulse for each IGBT of the four ones in each leg of the three-level dc/dc converter. The selection of the appropriate states that command the chopper is a function of the dc-bus voltage unbalance measured through $V_{\rm NP}$, and hence, of the contribution of charge from capacitors C_{d1} and C_{d2}.

V. Digital Simulation Results

The test PS used to validate the full detailed modeling and control approaches of the proposed SMES device for dynamic PS security improvement is depicted in Fig. 6 as a single-line diagram. This electric power network implements a bulk PS providing a small MG including a variety of DER units (DG based on fossil and renewable fuels and the advanced SMES) and different types of loads (DR). The small MG implements a dynamically-modeled double generator-type DG linked to a utility system represented by a classical single machine-infinite bus-type (SMIB) system. The first microgenerator is composed of a dispatchable unit powered by a typical gas microturbine directly coupled to a synchronous generator and includes a voltage regulator and a speed governor [31]. The second generator is made up of a variable-speed wind turbine generator developed using a direct-in-line system built with a direct-driven permanent-magnet synchronous generator (PMSG) grid-connected via a full-scale power converter [32]. The test MG implements an automatic load frequency control. This basic 12-bus network operates at 120 kV/50 Hz in the bulk system side and at 25 kV in the MG side, and implements a 100-MVA short circuit power level infinite bus through a Thevenin equivalent. Two sets of sheddable linear loads, grouped respectively at buses 10 and 11, are modeled as constant impedances. An MG central breaker (MGCB) with automatic reclosing capabilities is employed for the interconnection of the MG PCC (bus 5) to the bulk power network through a 20-km tie line. This high-speed grid separation device is implemented via a solid state circuit breaker (static transfer switch), and is used to rapidly disconnect the MG from the faulted bus under all conditions. The proposed SMES device representing the MG DES is placed at bus 5 (PCC) and includes a 25-kV/1.2-kV step-up transformer with a ±2-MVA/2.5-kV dc-bus PCS and a 1-MW/20-MJ SMES. Major data of the test PS including the SMES unit are summarized in the Appendix.

The dynamic performance of the proposed SMES device is assessed through digital simulations carried out in the MATLAB/Simulink environment [33], by using SPSs and C++ codes. To this aim, the SMES system is firstly charged to be initialized at half capacity, i.e., at 10 MJ with $I_{\rm sc}$ around 845 A and then the system is changed to the standby mode. Thus, both control

modes of the SMES device, i.e., VCM and FCM, are analyzed using three case studies relative to basic protection and operation of the MG, permitting to carry out both a large and a small-signal performance study of the SMES, besides the MG tie-line power flow stabilization and control.

The first case study (Scenario 1), which corresponds to a severe disturbance such as the MG island operation mode, considers a permanent fault that needs to be isolated by the instantaneous trip operation of the MGCB. A three-phase-to-ground fault is applied at bus 3 in the utility system at $t = 0.1$ s, and cleared 10 cycles later (200 ms) by tripping the tie line through the opening of the main MG circuit breaker. An automatic load-shedding protection scheme (LSPS) with ten frequency steps and a total load rejection of 1.4 MW is included at loads in order to prevent the system frequency collapse during this severe disturbance, but also to make use of the activated steps, and consequently, the rejected load as a performance comparison index for various scenarios with and without the inclusion of the SMES system. The second case study (Scenario 2), which represents a quite less severe disturbance than the prior case, such as power oscillations (swings) damping, assumes that the fault is temporary and implements an instantaneous trip action with automatic breaker reclosing at a preset delay time of 200 ms. The third case study (Scenario 3), considers the stabilization and control of the MG tie-line power flow when there is high penetration of wind generation. This inherently unpredictable and highly variable generation causes fluctuations of tie-line power flow that significantly affects the whole PS operation.

A. Scenario 1: Assessment of MG Operation in Island Mode

A major goal in designing an MG is to maintain uninterrupted power to critical loads. Thus, the ability of an MG to form intentional islands is assured by appropriately operating the DG systems located downstream of the main MGCB jointly with the DES and loads. To this aim, the proposed test MG is intentionally forced to operate in island mode at $t = 0.3$ s and the MG performance during the electrical island starting is analyzed through the simulation results shown in Fig. 7 with black dashed lines. For the configuration presented in the test case prior to the fault in steady state, i.e., during normal operation in which the MG is connected to the bulk PS, the gas microturbine is dispatched at 1.2 MW, while the wind generator is disconnected. In these circumstances the active power demanded by loads is 2 MW so that the MG needs to import about 0.8 MW from the bulk PS. In this interconnected operation, the MG frequency is at its rated value (1 p.u. of 50 Hz) and the voltage at bus 5 (PCC) is 0.97 p.u. (base voltage of 25 kV). After the fault is cleared and the tie-line tripped, the DG system is operated in island conditions. Under these circumstances, the microturbine itself has to supply all the power required by loads. As can be seen from the simulation results shown with black dashed lines for this base case with no DES, the gas microturbine respond slowly and is virtually inertia-less. The spinning reserve of the unit is neither sufficiently large nor fast enough for supporting the MG frequency, and thus, avoiding the islanded MG collapse. The activation of the automatic LSPS with six frequency steps

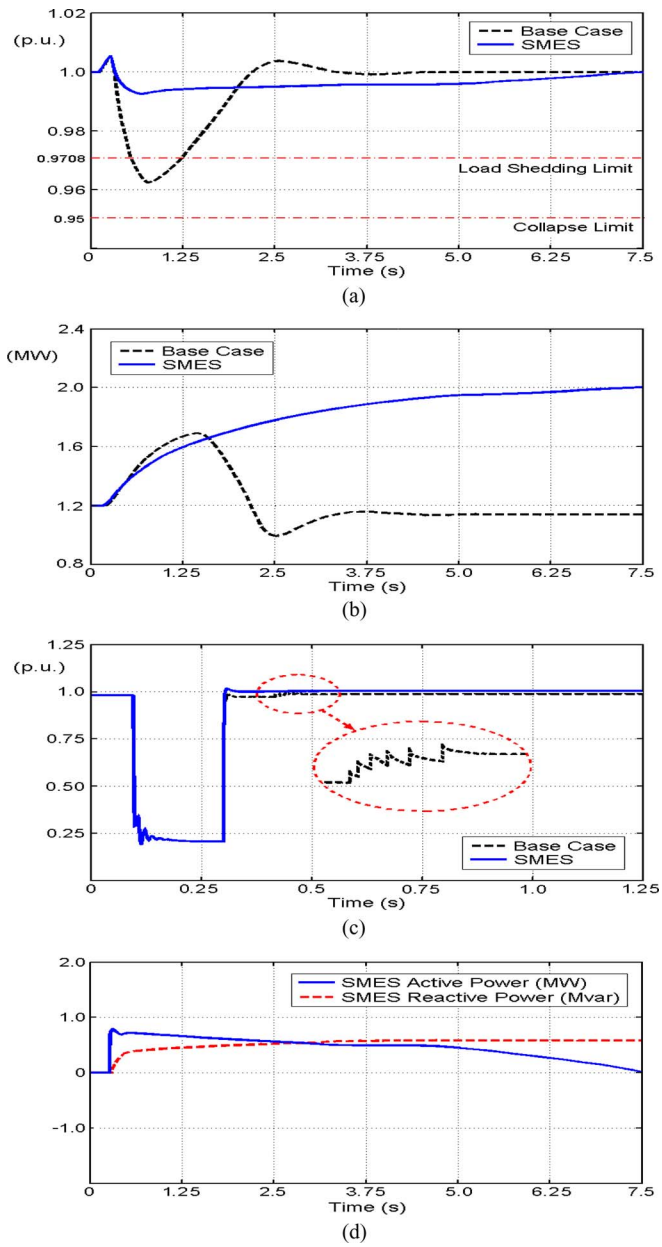

Fig. 7. Dynamic response of the MG in island mode (scenario 1). (a) System frequency. (b) Microturbine mechanical power. (c) PCC terminal voltage (bus 5). (d) SMES active and reactive power.

(see Fig. 7(c)) and a total load rejection of around 0.84 MW is required in order to recover the MG frequency to its scheduled value. Under this situation, the isolated system experiences a common low-frequency mode of about 0.27 Hz. The gas microturbine must be able to ramp up very fast in order to decrease the amount of load rejected, and to ramp down quickly for reducing the frequency deviation overshoot and settling time after the demand is stabilized, as can be derived from the microturbine mechanical power. Under these circumstances, the required demand cannot be fully satisfied bringing technical and economic consequences that are related to costs of deficits. Load rejection also permits to improve the steady-state voltage profile at bus 5

with each load shedding step activated, until reaching 0.986 V in steady state.

The effect of incorporating a ±2-MVA/1-MW/20-MJ SMES can be studied through the simulation results shown in Fig. 7 with blue solid lines. These results clearly show the outstanding dynamic performance of the SMES device. The rapid active power supplied by the SMES quickly absorbs the sudden power loss occurred after the tie-line tripping, and thus, enhances the damping of low-frequency oscillations. This condition permits to greatly decrease the power strain of the gas microturbine, since the generator is able to find the balance with the load at a lower speed than in the previous test case without producing a significant frequency deviation, resulting in a much smoother variation of the mechanical power of the machine, and thus, in an improvement of the reliability of the PS. In this case, the effects of the disturbance are totally mitigated in a shorter time than in the base case (black dashed lines) without being necessary to activate the LSPS. In fact, the frequency drop is drastically reduced and maintained far away from the load shedding limit. The minimum frequency reached during the disturbance is 0.992 p.u. (shown with blue solid lines) versus 0.962 p.u. for the base case (shown with black dashed lines). The improvement of the frequency control is obtained by the immediate action of the SMES coil for supplying/absorbing active power, which provides active power for about 7.5 s (approximately 4.6 MJ of energy). In this case, the SMES current I_{sc} is reduced from 845 A (10 MJ) to about 620 A (5.4 MJ) after 7.5 s. Furthermore, the capacitive reactive power locally generated by the SMES (maximum 0.55 Mvar) allows quickly regulating the voltage at bus 5 around the reference voltage of 1 p.u. (25 kV).

B. Scenario 2: Assessment of MG Operation in Interconnected Mode to a Faulted Feeder

The performance of the MG aiming at damping power flow oscillations in interconnected operation is now analyzed through the simulation results of Fig. 8, for the base case (i.e., with no DES) shown with black dashed lines. The disturbance occurring in the bulk PS after the fault clearance and subsequent automatic reclosing of the MGCB causes electromechanical oscillations of the gas microturbine generator. These local oscillations between the electrical machine and the rest of the utility system must be effectively damped to maintain the MG stability. As can be noted from digital simulations, a local mode of approximately 1.82 Hz that settles down to its steady state value after 2 s is induced in the MG. As expected, this low frequency power swing influences not only the MG frequency and the microturbine rotor angle deviation, but also the voltage profile at bus 5 (mean value of 0.97 p.u.).

The effect of incorporating the improved SMES system can be verified through the simulation results shown in Fig. 8 with blue solid lines. The transient response clearly proves the outstanding small-signal dynamic performance of the proposed MBS of the SMES device. The SMES unit acts as an efficient damper, absorbing surplus energy from the system and releasing energy at the appropriate time. The SMES unit with the proposed controller is capable of damping the oscillations in a short time

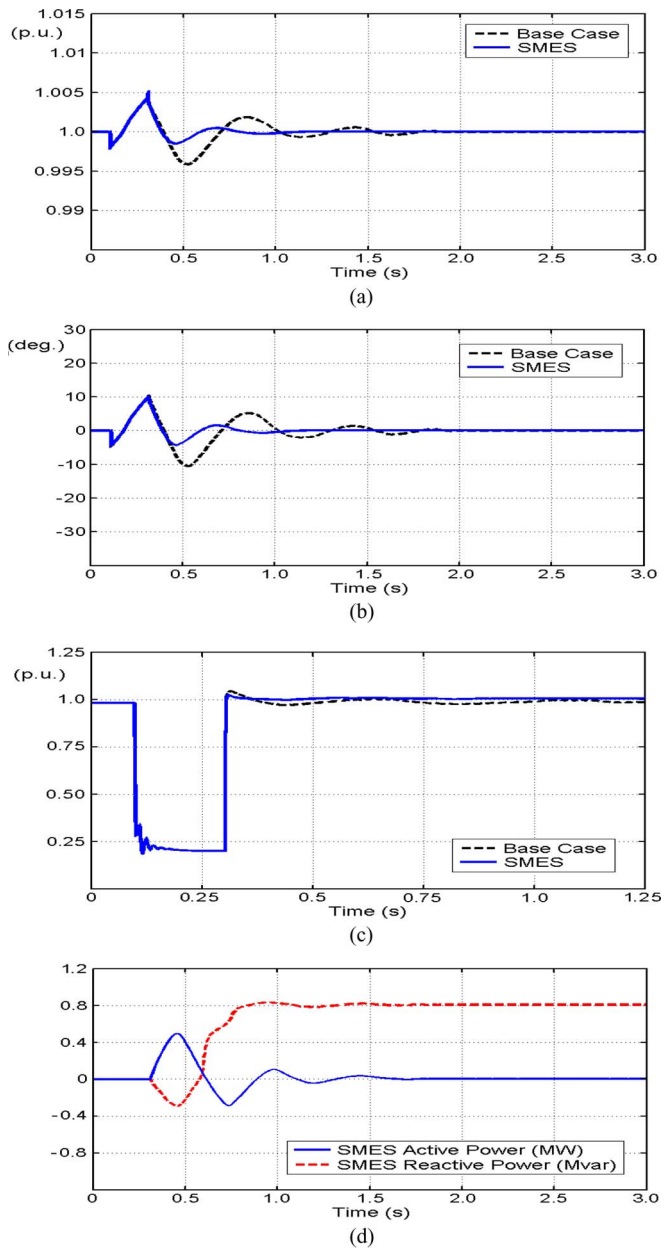

Fig. 8. Dynamic response of the MG in power flow oscillations damping mode (scenario 2). (a) System frequency. (b) Microturbine rotor angle deviation. (c) PCC terminal voltage (BUS 5). (d) SMES active and reactive power.

and reducing considerably the amplitude of the pulsations on the frequency. In the present analysis, the settling time for the MG frequency is about 0.78 s when the SMES unit is used for active and reactive power compensation employing the MBS controller. Furthermore, the frequency and rotor angle deviations are greatly reduced to values lesser than the maximum reached at the end of the fault when exists the peak increase in the kinetic energy of the microturbine. A noteworthy point is that the energy capacity rating of the SMES unit used in this case study for damping low frequency power swings is only 0.20 MJ with a maximum power rating of almost 0.56 MW. In this case, the SMES current I_{sc} is reduced from 845 A (10 MJ) to a bit less than 837 A (9.8 MJ) after 2 s. In addition, the rapid exchange

of capacitive reactive power with the MG (0.8 Mvar in steady state) allows the SMES to regulate (stabilize and support) the voltage profile at bus 5.

C. Scenario 3: Assessment of MG Operation with High Penetration of wind Generation

The performance of the MG in interconnected operation and with high penetration of wind generation is now analyzed through the simulation results of Fig. 9, for the base case (i.e., with no DES) shown with black dashed lines. Real data of wind profile during 300 s have been measured and digitalized to represent the input of the 1.8 MW wind power generator. Under standard conditions, the wind generator produces the fluctuating active power profile shown with black solid lines. Under these circumstances, the MG tie line to the bulk PS is subjected to considerably variable power that significantly affects the operation of both the MG and the bulk PS. Since the gas microturbine is disconnected in this case study, all loads are provided by the wind generator alone so that the power imported from the bulk PS is highly fluctuating between 0.5 and 1.5 MW for balancing the approximately 2 MW demand. In these conditions, the voltage at bus 5 (PCC) is also influenced and fluctuates around a mean value of 0.978 p.u. (of 25 kV), as shown with black dashed lines.

The consequence of including the proposed SMES system can be verified through the simulation results shown in Fig. 9 with blue solid lines. The transient response clearly proves the outstanding dynamic performance of the proposed MBS controller of the SMES device. The SMES effectively stabilize the tie-line power flow, absorbing surplus energy from the system and releasing energy at the appropriate time. Thus, the tie-line power flow with the SMES active power compensation slightly fluctuates around 1 MW in this case and the wind power generation with the proposed DES acts as an overall near dispatchable RES-based DG unit. In this way, the maximum and minimum tie-line power flow is greatly restricted and therefore the line capacity is maximized. The energy capacity rating of the SMES unit employed in this scenario is only around 0.33 MJ with a power rating of nearly 0.5 MW. In this case, the SMES current I_{sc} is reduced from 845 A (10 MJ) to nearly 831 A (9.67 MJ) after 5 min. Moreover, the capacitive reactive power locally generated by the SMES (average 0.35 Mvar) allows quickly supporting and controlling the voltage at bus 5 around the reference voltage of 1 p.u. (25 kV).

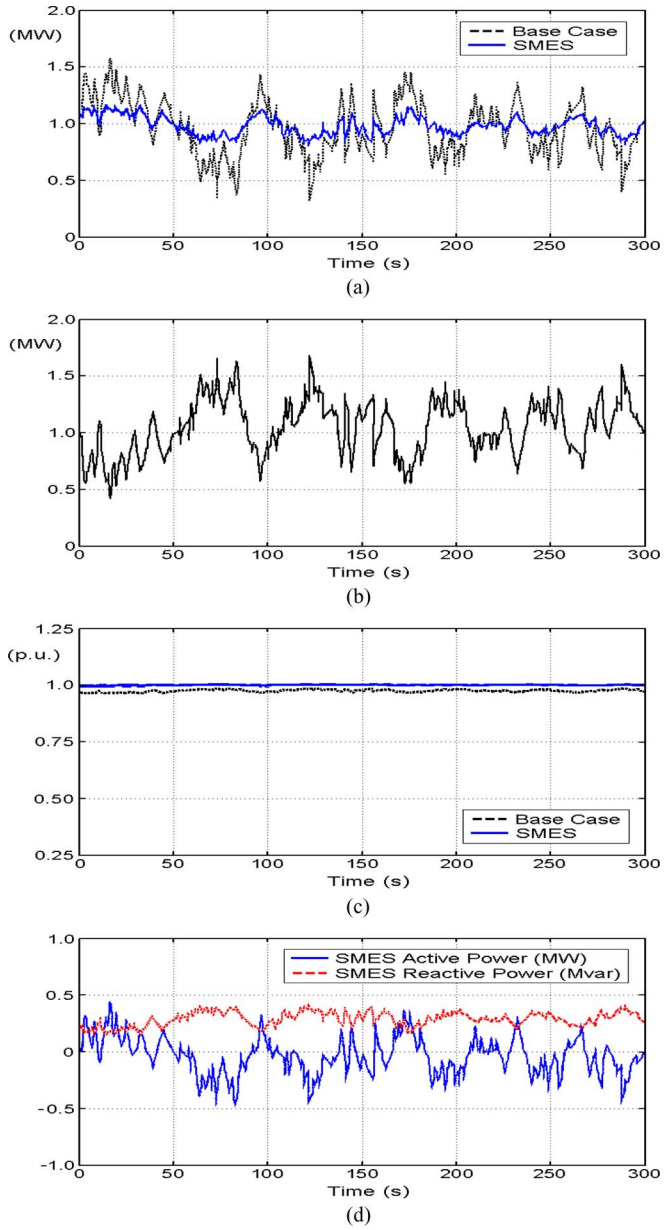

Fig. 9. Dynamic response of the MG in grid tie-line power flow stabilization and control mode (scenario 3). (a) MG tie-line power flow. (b) Wind turbine generator active power. (c) PCC terminal voltage (bus 5). (d) SMES active and reactive power.

VI. Preliminary Experimental Results

In order to verify the validity of the proposed PCS of the SMES and its control scheme, a 3-kVA laboratory-scale prototype was designed and implemented. The VSI was built with IGBTs with internal antiparallel diodes, and fast clamping diodes. The VSI was designed to operate at 5 kHz and is connected to the 50 Hz frequency utility grid at the 380-V line voltage level through the inductive–capacitive low-pass filter and three 220/60 V step-up coupling transformers connected in a Yg/Δ configuration. Since the SMES coil has a quite large inductance, its behavior was roughly emulated using a controlled 20 A dc current source. The bidirectional dc/dc converter interfacing the current source to the 80 V dc bus of the VSI was designed to operate at 5 kHz and also built with IGBTs and fast diodes.

The proposed three-level control scheme was entirely implemented on a high-performance 32-bit fixed-point Texas Instruments TMS320F2812 digital signal processor (DSP) operating at 150 MHz and residing on an eZDSPF2812 evaluation board. This processor includes an advanced 12-bit analog-to-digital converter (ADC) with a fast conversion time that makes it possible real-time sampling with high accuracy and real-time *abc* to synchronous *d–q* frame coordinate transformation, so that the proposed multiobjective control block can be successfully

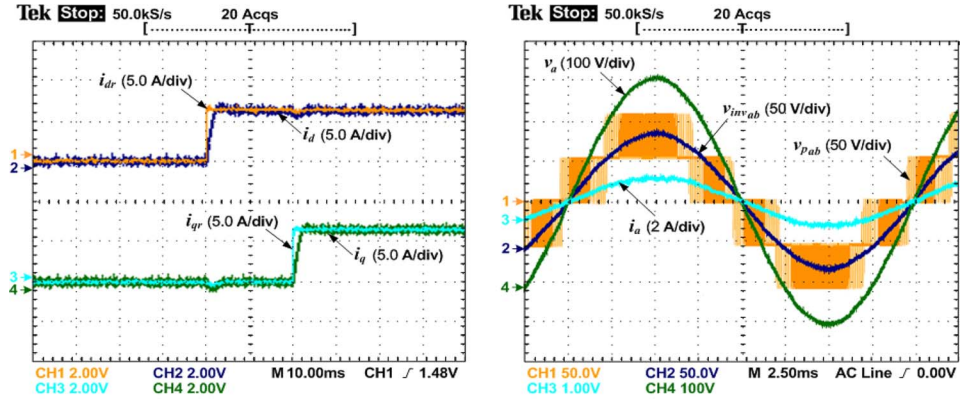

Fig. 10. SMES actual output response: (a) d–q coordinates output currents in the time domain for a step change in the active and reactive power provided to the MG, (b) steady-state voltage and current waveforms during active power exchange.

TABLE II
BULK PS PARAMETERS

Three-phase ac source				Coupling transformer					
Rated voltage (kV)	Freq. (Hz)	S.C. level (MVA)	X/R	S_{max} (MVA)	Voltage relation (kV/kV)	R (p.u.)	X (p.u.)	G (p.u.)	B (p.u.)
120	50	100	10	100	120/25	0.0033	0.05	0.0012	0.0023

TABLE III
MG PARAMETERS

Tie line (B3-B4)				Lines (B5-B6, B5-B8)				Coupling transformers (all loads)					
L (km)	R (p.u.)	X (p.u.)	B (p.u.)	L (km)	R (p.u.)	X (p.u.)	B (p.u.)	S_{max} (MVA)	Voltage relation (kV/kV)	R (p.u.)	X (p.u.)	G (p.u.)	B (p.u.)
20	0.0062	0.034	0.081	5.0	0.0016	0.0082	0.021	2.0	25/0.38	0.0013	0.015	0.0003	0.0006

carried out. The DSP was operated with a selected sample rate of 160 ksps and low-pass filters were implemented using fifth-order low-pass filters based on a Sallen and Key designs. The control pulses for the VSI and the chopper were generated by employing two DSP-integrated pattern generators (event managers). The gate driver board of the IGBTs was designed to adapt the wide differences of voltage and current levels with the DSP and to provide digital and analog isolation using optically coupled isolators. All the source code was written in C++ by using the build-in highly efficient DSP compiler. A digital real-time oscilloscope (Tektronix TPS2024) was used to display and capture the required output waveforms.

The experimental results of the proposed controller in simultaneous active and reactive power control are shown in Fig. 10. In this case, the external-level control was reduced to a general active and reactive power command to achieve the desired system dynamic response and therefore to simplify the experiment. Dc time domain waveforms for the PCS prototype with step changes of approximately 500 W and 500 var are provided. As can be noted, the independent nature of the control is evident since the change in the output direct current of around 6.25 A (providing the active power) causes a small response in the quadrature output current (giving the reactive power) and vice versa. These results obtained from small-scale experiments are in good agreement with results provided by simulations at the same operating conditions. Nevertheless, some differences would be expected within a noisy environment of real high-power SMES systems. Further performance tests will be carried out with a real higher capacity HTS SMES prototype included into an MG, both being currently developed.

VII. CONCLUSION

This paper has presented an effective SMES controller for the stabilization and control of the power flow of a hybrid MG with high penetration of wind generation. A novel PCS of the SMES unit to simultaneously and independently control active and reactive power flow has been studied and implemented. A real detailed full model and a novel multilevel control algorithm based on a decoupled current control strategy in the synchronous-rotating $d-q$ reference frame with a novel controller to prevent dc-bus capacitors voltage drift/imbalance were proposed. The control system employs a flexible MBS controller for power damping in the frequency range of up to 4 Hz. The novel multilevel control scheme ensures fast controllability of the SMES operating in the four-quadrant modes, which enables to effectively increase the transientand dynamic stability of the MG.

TABLE IV
MG PARAMETERS (CONT.)

Coupling transformers (all DG units)						Loads (B10, B11)					LSPS (10 steps)		
S_{max} (MVA)	Voltage relation (kV/kV)	R (p.u.)	X (p.u.)	G (p.u.)	B (p.u.)	Voltage (kV)	P_{L1} (MW)	Q_{L1} (Mvar)	P_{L2} (MW)	Q_{L2} (Mvar)	Freq. step (Hz)	Load rejection/step (MW/Mvar)	Activation limit (Hz)
3.0	25/1.8	0.0023	0.019	0.0007	0.0009	0.38	1.5	0.35	0.5	0.11	0.0056	0.14/0.02	0.9708

TABLE V
DG UNITS PARAMETERS

Gas microturbine					Direct-driven PMSG wind turbine					
Rated power (MVA)	Rated voltage (kV)	P_G (MW)	Q_G (Mvar)	Inertia constant H (MW/MJ)	Rated power (MVA)	Rated voltage (kV)	P_G (MW)	Q_G (Mvar)	Dc link voltage (kV)	Inertia constant H (MW/MJ)
2.1	1.8	2.0	0.64	0.65	2.0	1.8	1.8	0.87	2.5	0.62

TABLE VI
SMES SYSTEM DATA

Coupling transformer						VSC				Chopper and SMES coil			
S_{max} (MVA)	Voltage relation (kV/kV)	R (p.u.)	X (p.u.)	G (p.u.)	B (p.u.)	Rated power (MVA)	Q_{max} (Mvar)	Dc link voltage (kV)	C_{d1}, C_{d2} (mF)	P_{max} (MW)	$E_{SC,max}$ (MJ)	$I_{SC,max}$ (kA)	$V_{SC,max}$ (kV)
2.0	25/1.2	0.0022	0.017	0.0006	0.00085	2.0	1.7	2.5	2.2	1.0	20	1.2	3.2

TABLE VII
SMES COIL MODEL DATA

# Seg.	L_i (H)	M_{ij} (H)	C_{Si} (μF)	C_{Shi} (μF)	R_{pi} (Ω)	R_p (Ω)	C_{S1}, C_{S2} (μF)	R_{g1}, R_{g2} (kΩ)	C_F (μF)
6	4.67	1.12	0.006	0.237	0.024	2.55	0.6	13.5	3.5

TABLE VIII
SMES CONTROLLER PARAMETERS

External level data																						Middle level data			
K_{p1}	K_{I1}	R_d, R_p	K_v	T_1, K_{L1}	T_2	K_{vf}	K_{HF}, C, E	K_L, D	K_H	K_{p2}	K_L, K_{I2}	T_{I1}	T_{I2}, T_{I3}	T_{I4}	T_{H1}	T_{H2}, T_{H3}	T_{H4}	K_{I1}, K_{I2}	K_{H1}, K_{H2}	T_{L1F}	A	B	K_{p3}, K_{p4}	K_{I3}, K_{I4}	K_{p5}	K_{I5}
3.0	35	0.05	1.0	1.2	6.7	0.7	80	125	250	5.0	30	0.13	0.16	0.19	0.015	0.018	0.022	32	67	-1.76e-3	1.274	1.78e-2	3.5	12	0.01	65

APPENDIX

See Tables II–VIII.

REFERENCES

[1] J. M. Guerrero, F. Blaabjerg, T. Zhelev, K. Hemmes, E. Monmasson, S. Jemei, M. P. Comech, R. Granadino, and J. I. Frau, "Distributed generation: Toward a new energy paradigm," *IEEE Ind. Electron. Mag.*, vol. 4, no. 1, pp. 52–64, Mar. 2010.

[2] N. Hatziargyriou, H. Asano, R. Iravani, and C. Marnay, "Microgrids," *IEEE Power Energy Mag.*, vol. 5, no. 4, pp. 78–94, Jul./Aug. 2007.

[3] B. Kroposki, R. Lasseter, T. Ise, S. Morozumi, S. Papatlianassiou, and N. Hatziargyriou, "Making microgrids work," *IEEE Power Energy Mag.*, vol. 6, no. 3, pp. 40–53, May/Jun. 2008.

[4] J. M. Guerrero, J. C. Vasquez, J. Matas, M. Castilla, and L. García de Vicuña, "Control strategy for flexible microgrid based on parallel line-interactive UPS systems," *IEEE Trans. Ind. Electron.*, vol. 56, no. 3, pp. 726–736, Mar. 2009.

[5] F. Katiraei, R. Iravani, N. Hatziargyriou, and A. Dimeas, "Microgrids management: Controls and operation aspects of microgrids," *IEEE Power Energy Mag.*, vol. 6, no. 3, pp. 40–53, May/Jun. 2008.

[6] F. Blaabjerg, R. Teodorescu, M. Liserre, and A. V. Timbus, "Overview of control and grid synchronization for distributed power generation systems," *IEEE Trans. Ind. Electron.*, vol. 53, no. 5, pp. 1398–1409, Oct. 2006.

[7] J. M. Guerrero, L. Hang, and J. Uceda, "Control of distributed uninterruptible power supply systems," *IEEE Trans. Ind. Electron*, vol. 55, no. 8, pp. 2845–2859, Aug. 2008.

[8] S. Rahman, "Going green: The growth of renewable energy," *IEEE Power Energy Mag.*, vol. 1, no. 6, pp. 16–18, Nov./Dec. 2003.

[9] I. Serban and C. Marinescu, "Power quality issues in a stand-alone microgrid based on renewable energy," *Revue Roumaine des Sci. Tech., Série Électrotech. Énergétique*, vol. 53, no. 3, pp. 285–293, Jun./Sep. 2008.

[10] I. Serban, R. Teodorescu, J. M. Guerrero, and C. Marinescu, "Modeling of an autonomous microgrid for renewable energy sources integration," in *Proc. 35th Annu. Conf. IEEE Ind. Electron. Soc. (IECON 2009)*, Nov., pp. 4311–4316.

[11] M. H. Ali, B. Wu, and R. A. Dougal, "An overview of SMES applications in power and energy systems," *IEEE Trans. Sust. Energy*, vol. 1, no. 1, pp. 38–47, Apr. 2010.

[12] M. G. Molina, P. E. Mercado, and E. H. Watanabe, "Static synchronous compensator with superconducting magnetic energy storage for high power utility applications," *Energy Conv. Manage.*, vol. 48, no. 8, pp. 2316–2331, Aug. 2007.

[13] M. G. Molina and P. E. Mercado, "Control design and simulation of DSTATCOM with energy storage for power quality improvements," in *Proc. 2006 IEEE/PES Transmiss. Distrib, Conf, Expo.*, Latin America, Aug. 2006, pp. 1–8.

[14] F. Blaabjerg, Z. Chen, and S. Kjaer, "Power electronics as efficient interface in dispersed power generation systems," *IEEE Trans. Power Electron.*, vol. 19, no. 5, pp. 1184–1194, Sep. 2004.

[15] J. Rodriguez, J. S. Lai, and F. Z. Peng, "Multilevel inverters: A survey of topologies, controls, and applications," *IEEE Trans. Ind. Electron.*, vol. 49, no. 4, pp. 724–738, Aug. 2002.
[16] J. M. Carrasco, L. G. Franquelo, J. T. Bialasiewiez, E. Galvan, R. C. P. Guisado, M. A. M. Prats, J. I. Leon, and N. Moreno-Alfonso, "Power-electronic systems for the grid integration of renewable energy sources: A survey," *IEEE Trans. Power Electron.*, vol. 53, no. 4, pp. 1002–1016, Aug. 2006.
[17] A. Von Jouanne, S. Dai, and H. Zhang, "A multilevel inverter approach providing DC-link balancing, ride-through enhancement, and common-mode voltage elimination," *IEEE Trans. Ind. Electron.*, vol. 49, no. 4, pp. 739–745, Nov. 2002.
[18] A. B. Arsoy, Y. Liu, P. F. Ribeiro, and F. Wang, "STATCOM-SMES," *IEEE Ind. App. Mag.*, vol. 9, no. 2, pp. 21–28, Mar./Apr. 2003.
[19] A. Kwasinski, "Identification of feasible topologies for multiple-input dc-dc converters," *IEEE Trans. Power Electron.*, vol. 24, no. 3, pp. 856–861, Mar. 2009.
[20] C. K. Sao and P. W. Lehn, "Control and power management of converter fed microgrids," *IEEE Trans. Power Syst.*, vol. 23, no. 3, pp. 1088–1098, Aug. 2008.
[21] M. V. Aware and D. Sutanto, "SMES for protection of distributed critical loads," *IEEE Trans. Power Del.*, vol. 19, no. 3, pp. 1267–1275, Jul. 2004.
[22] L. Chen, Y. Liu, A. B. Arsoy, P. F. Ribeiro, M. Steurer, and M. R. Iravani, "Detailed modeling of superconducting magnetic energy storage (SMES) system," *IEEE Trans. Power Del.*, vol. 21, no. 2, pp. 699–710, Apr. 2006.
[23] M. Steurer and W. Hribernik, "Frequency response characteristics of a 100 MJ SMES coil—Measurements and model refinement," *IEEE Trans. Appl. Supercond.*, vol. 15, no. 2, pp. 1887–1890, Jun. 2005.
[24] J. Sun, "Small-signal methods for ac distributed power systems—A review," *IEEE Trans. Power Electron.*, vol. 24, no. 11, pp. 2545–2554, Nov. 2009.
[25] E. Barklund, N. Pogaku, M. Prodanovic, C. Hernández-Aramburo, and T. C. Green, "Energy management in autonomous microgrid using stability-constrained droop control of inverters," *IEEE Trans. Power Electron.*, vol. 23, no. 5, pp. 2346–2352, Sep. 2008.
[26] A. Timbus, M. Liserre, R. Teodorescu, P. Rodriguez, and F. Blaabjerg, "Evaluation of current controllers for distributed power generation systems," *IEEE Trans. Power Electron.*, vol. 24, no. 3, pp. 654–664, Mar. 2009.
[27] M. G. Molina and P. E. Mercado, "Control of tie-line power flow of microgrid including wind generation by DSTATCOM-SMES controller," in *Proc. 2009 Energy Conv. Congr. Expo. (ECCE 2009)*, Sep., pp. 2014–2021.
[28] E. Twining and D. G. Holmes, "Grid current regulation of a three-phase voltage source inverter with an LCL input filter," *IEEE Trans. Power Electron.*, vol. 18, no. 3, pp. 888–895, May 2003.
[29] Y.-F. Liu, E. Meyer, and X. Liu, "Recent developments in digital control strategies for dc/dc switching power converters," *IEEE Trans. Power Electron.*, vol. 24, no. 11, pp. 2567–2577, Nov. 2009.
[30] Y. Wenxi, H. Haibing, and L. Zhengyu, "Comparisons of space-vector modulation and carrier-based modulation of multilevel inverter," *IEEE Trans. Power Electron.*, vol. 23, no. 1, pp. 45–51, Jun. 2008.
[31] A. K. Saha, S. Chowdhury, S. P. Chowdhury, and P. A. Crossley, "Modeling and performance analysis of a microturbine as a distributed energy resource," *IEEE Trans. Energy Conv.*, vol. 24, no. 2, pp. 529–538, Jun. 2009.
[32] R. Teodorescu and F. Blaabjerg, "Flexible control of small wind turbines with grid failure detection operating in stand-alone and grid-connected mode," *IEEE Trans. Power Electron.*, vol. 9, no. 5, pp. 1323–1332, Sep. 2004.
[33] (2009). SimPowerSystems for use with Simulink: User's Guide, updated for Simulink v7.3. The MathWorks, Inc., Natick, MA [Online]. Available at: http://www.mathworks.com/

Marcelo Gustavo Molina (S'01–M'05) was born in San Juan, Argentina. He received the Graduate degree in electronic engineering and the Ph.D. degree from the National University of San Juan (UNSJ), San Juan, in 1997 and 2004, respectively.

During 2004, he was a Doctoral Research Fellow at the Federal University of Rio de Janeiro, Brazil, supported by Coordinación de Perfeccionamiento del Personal del Nivel Superior (CAPES). From 2005 to 2007, he was a Postdoctoral Research Fellow with the Argentinean National Council for Science and Technology Research (CONICET), UNSJ. In 2009, he was a Visiting Professor at the University of Siegen, Siegen, Germany, sponsored by Deutscher Akademischer Austausch Dienst (DAAD), and in 2010 at the Federal University of Rio de Janeiro, Brazil, supported by CAPES. Since 2004, he has been an Associate Professor at the UNSJ and a Researcher with the CONICET. His current research interests include new energy technologies, simulation methods, power systems dynamics and control, power electronics modeling and design, renewable energy resources and the application of energy storage in power systems.

Dr. Molina is a member of the IEEE Power Engineering Society and the Power Electronics Society.

Pedro Enrique Mercado (M'02–SM'02) was born in San Juan, Argentina. He received the Graduate degree in electromechanical engineering from the National University of San Juan (UNSJ), San Juan, Argentina, and the Ph.D. degree from the Aachen University of Technology (RWTH), Aachen, Germany.

He is currently a Professor of electrical engineering at the UNSJ and a Researcher at the Argentinean National Council for Science and Technology Research (CONICET), Buenos Aires, Argentina. His current research research interests include operation security, power electronics, renewable energy systems, and economic operation and control of electric power systems.

Dr. Mercado is a Senior Member of the IEEE Power Engineering Society and the Power Electronics Society.